Bitlis Eren Üniversitesi Fen Bilimleri Dergisi
BİTLİS EREN UNIVERSITY JOURNAL OF SCIENCE
ISSN: 2147-3129/e-ISSN: 2147-3188
VOLUME: 13 NO: 1 PAGE: 62-78 YEAR: 2024
DOI:10.17798/bitlisfen.1332971

Imidazole Based Novel Schiff Base: Synthesis, Characterization, Quantum Chemical Calculations, In Silico Investigation of ADMEt Properties and Molecular Docking Simulations against VEGFR2 Protein

Ömer DİLEK*

Isparta University of Applied Sciences, Central Research Laboratory Application and Research Center, 32200, Isparta, Turkey
(ORCID: 0000-0003-1409-782X)

Keywords: Schiff base, Imidazole, ADMEt, DFT, Molecular docking

Abstract

The potential drug candidate novel Schiff base, 2-(((3-(4-methyl-1H-imidazol-1-yl)-5-(trifluoromethyl)phenyl)imino)methyl)phenol (MITPIM) was synthesized by using salicylaldehyde and 1-[3-Amino-5-(trifluoromethyl)phenyl]-4-methylimidazole, the precursor of nilotinib used in cancer treatment. It was characterized by using spectroscopic techniques such as ^{1}H-NMR, ^{13}C-NMR, ^{19}F-NMR, FT-IR, and UV-Vis. DFT computational technique was used for further investigation. DFT/B3LYP method and the 6-311G(d,p) basis set were used to determine optimized geometry. Then by using optimized geometry and DFT approach three-dimensional molecular electrostatic potential (MEP), vibration frequencies, NMR chemical shift values, HOMOs-LUMOs, and molecular orbital energies were calculated. It was noted that there was good agreement between the experimental and theoretical findings. The ADME and toxicity properties were investigated by using online servers. It was determined from the findings that the MITPIM had good oral bioavailability and minimal toxicity. By using 2XIR protein, the molecular docking simulations of MITPIM were also investigated. The binding energy of the MITPIM-2XIR complex was determined as −9.34 kcal/mol. It was close to nilotinib's binding energy which was −9.69 kcal/mol. Molecular docking and ADMEt results show that the newly synthesized MITPIM has the potential to be a drug.

1. Introduction

Cancer is a type of disease that is caused by cells with the ability to divide uncontrollably, has the potential to spread to other tissues of the body, is the second leading cause of death [1], and is responsible for one out of every 6 deaths worldwide [2], which profoundly affects the individual materially and spiritually. Current treatment methods are surgery, radiotherapy, chemotherapy, hormonal, and targeted drug therapy [2] Due to the undesirable side effects of existing chemotherapeutic drugs and radiotherapy methods, studies on the synthesis of new, easy-to-access, low-cost, targeted anticancer drugs and investigation of their antiproliferative properties have increased [3] nowadays.

When the structures of drug molecules used in cancer treatments in recent years are examined, it is seen that these molecules contain heterocyclic units in their structures. Heterocyclic compounds are structures that have an important place in organic chemistry, containing at least one heteroatom such as nitrogen (N), oxygen (O), or sulfur (S) unlike the carbon atom in their structure. These structures contribute greatly to medicinal chemistry because of their wide application in drug discovery and development [4–6]. The heterocyclic imidazole ring has an aromatic structure containing two nitrogen atoms in its structure, showing polar properties, being

* Corresponding author: omerdilek@isparta.edu.tr
Received: 26.07.2023, Accepted: 09.01.2024

easily ionizable, soluble in water and other polar solvents, and showing amphoteric properties. Because of these properties, the imidazole ring increases the pharmacokinetic properties of the molecule it is found in and is therefore used to optimize the solubility and bioavailability parameters of the molecules [7]. Fluorine (F) is the smallest substituent that can replace the hydrogen atom in organic chemistry. The replacement of hydrogen atoms with fluorine atoms is widely used in medicinal chemistry. The main reasons for this are fluorine has strong electron-withdrawing properties, electrostatic interactions, small atomic size, and high lipophilicity. Additionally, electrostatic interactions of fluorine atoms with proteins, facilitate the binding of ligands to proteins. Synthesis of fluorine-containing molecules and biological applications of them, primarily those with the $-CF_3$ group, are growing daily. [8–10]. Phenolic compounds with OH functional groups have an important place in medicinal chemistry because they have antioxidant, anticancer, antiviral, insecticidal, antimicrobial, and antiparasitic activities [6], [11–13]. Schiff bases are substances that have an imine or azomethine functional group. In the design and development of numerous bioactive lead compounds, it has been discovered that Schiff bases are flexible pharmacophores. Schiff bases have biological activities such as anti-inflammatory, analgesic, antimicrobial, anticonvulsant, antitubercular, anticancer, antioxidant, anthelmintic, antiglycation, and antidepressant activities [14].

The low availability, high cost, and low number of drug agents used in cancer treatment have encouraged researchers to work towards finding new anticancer drugs that are easy to access and low in cost. For this purpose, computer-aided drug design methods have gained importance recently and studies on the design of new drugs with *in silico* techniques have increased. Because this technique not only examines the interaction of drugs with target proteins but also eliminates a large number of molecules and reduces the number of molecules to a minimum. It also shortens the molecule's time to become a drug. In addition, establishing of physicochemical, lipophilicity, water solubility, pharmacokinetic, and drug-likeness properties of new drug candidates by using *in silico* techniques have a crucial role. For example, topological polar surface area (TPSA), Log $P_{o/w}$, Lipinski's rule of five, water solubility, gastrointestinal absorption, and some other properties are criteria sought in drug candidate molecules. These properties of new drug candidates can be learned in advance using *in silico* techniques.

The compound 1-[3-Amino-5-(trifluoromethyl)phenyl]-4-methylimidazole is the precursor of the nilotinib molecule used in cancer treatment. Additionally, this aniline and the compounds produced from it make it a viable substance for additional research and development in the field of pharmaceuticals [15–24]. Based on all of this knowledge, in this work the novel potential bioactive compound, 2-(((3-(4-methyl-1H-imidazol-1-yl)-5-(trifluoromethyl)phenyl)imino) methyl)phenol (MITPIM) which was derived from 1-[3-Amino-5-(trifluoromethyl)phenyl]-4-methylimidazole, was containing imidazole ring, a fluorine atom, imine, and the phenolic functional group was designed and then synthesized.

Spectroscopic techniques were used to identify MITPIM. All quantum chemical calculations were done by using 6-311G(d,p) basis set and DFT/B3LYP method. As a result of quantum chemical calculations. the theoretical vibrational frequencies, NMR chemical shifts, maximum absorption wavelengths, frontier orbitals and MEP surface diagram were obtained. By using VEGFR2 protein (PDB ID: 2XIR), the molecular docking simulations of MITPIM were investigated. ADME and toxicity properties of MITPIM were determined using the SwissADME and ProTox-II online servers.

2. Material and Method

2.1. Physical measurements

The chemicals were supplied by Merck and Aldrich Chemical Company. Chemicals were used without further purification. Aluminum sheets pre-coated with silica gel SIL G/UV254 from MN GmbH & Co., were used to follow reactions. The spots were made visible in UV light (254 nm). Melting point was measured in an open glass capillary tube by using an Electro-thermal 9100 apparatus. The values are not corrected. A Bruker NMR spectrometer (700 MHz) was used to record the ^{1}H and ^{13}C NMR spectra while a Varian NMR spectrometer (600 MHz) was used to record ^{19}F NMR spectrum. Chemical shifts are expressed as parts per million (ppm) in relation to the solvent's residual protons ($CHCl_3$: 7.26 ppm) and carbon resonance ($CDCl_3$: 77.00 ppm). The NMR peak multiplicities were as follows: s for singlet, d for doublet, t for triplet, q for quartet, m for multiplet. 1×10^{-4} M solution compound and PG T80+ double beam spectrophotometer were used to record UV-Vis spectra. The infrared (FT-IR) spectrum was recorded by using the Thermo Nicolet i10, ν_{max} in cm^{-1}.

2.2. Synthesis of 2-(((3-(4-methyl-1H-imidazol-1-yl)-5-(trifluoromethyl)phenyl)imino) methyl) phenol (3)

The route of synthesis is depicted in **Figure 1**. Round-bottomed and two necked flask was charged with 1-[3-Amino-5-(trifluoromethyl)phenyl]-4-methylimidazole [25] (**1**, 965.0 mg; 4.0 mmol; 1.0 eq) and salicylaldehyde (**2**, 489.0 mg; 4.0 mmol; 1.0 eq). A magnetic stirring bar and absolute ethanol (20 mL) were added into the flask, the reflux condenser was equipped and the neck was capped with the glass stopper. The mixture was heated up to 80 ˚C and was stirred overnight at this temperature under N_2. TLC technique was used to follow reaction convertion. After completion of the reaction, approximately half of the solvent was evaporated under nitrogen. The mixture was cooled to ambient temperature. The mixture was poured into the beaker containing 50 mL *n*-heptane and the beaker was left in a refrigerator at 4 °C overnight. The solids were filtered, cake was dried under a vacuum. The aimed title product **3** was synthesized by 80% yield (1.1 g, 3.19 mmol) as a white solid. **Mp:** 108-110 °C. **FT-IR** (KBr): ν_{max} (cm^{-1}) = 3360 (br), 2926 (w), 1610 (s), 1495 (s), 1468 (s), 1320 (s), 1287 (s), 1175 (s). **^{1}H NMR (700 MHz, $CDCl_3$):** δ = 12.50 (s, 1H), 8.66 (s, 1H), 7.85 (s, 1H), 7.51 (s, 1H), 7.47 – 7.38 (m, 4H), 7.09 (s, 1H), 7.05 (dd, *J* = 8.7, 0.6 Hz, 1H), 6.99 (td, *J* = 7.5, 1.0 Hz, 1H), 2.31 (d, *J* = 0.9 Hz, 3H). **^{13}C{^{1}H} NMR (176 MHz, $CDCl_3$):** δ = 165.34 (CH), 161.18 (C), 151.01 (C), 140.51 (C), 138.90 (C), 134.49 (CH), 134.42 (CH), [133.81, 133.62, 133.43, 133.24, (C, $J^2_{C\text{-}F}$ = 33.4 Hz)], 132.94 (CH), [125.44, 123.89, 122.34, 120.79, (C, $J^1_{C\text{-}F}$ = 273.2 Hz)], 119.54 (CH), 118.55 (C), 117.49 (CH), 117.10 (CH), [116.03, 116.00, (CH, $J^3_{C\text{-}F}$ = 3.7 Hz)], [115.35, 115.34, (CH, $J^3_{C\text{-}F}$ = 3.3 Hz)], 114.28 (CH), 13.65 (CH_3). **^{19}F NMR (CPD, 564 MHz, $CDCl_3$):** δ = -57.85. **UV-Vis ($CHCl_3$):** λ_1 = 248 nm, λ_2 = 272 nm, λ_3 = 344 nm.

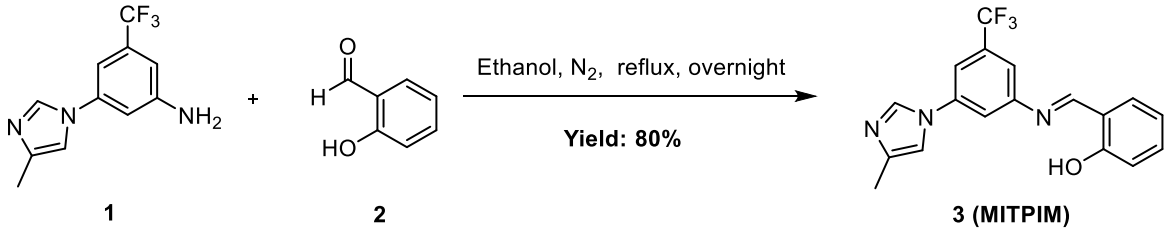

Figure 1. Synthesis of the compound MITPIM

2.3. Computational methods

Quantum chemical calculations were done by using Gaussian 09 package program [26]. Avogadro and Chemcraft were used for all visualizations of quantum chemical calculations [27], [28]. Optimized geometry of MITPIM was determined by using DFT/B3LYP/6-311G(d,p) approach [29], [30]. Calculated vibrational frequencies from optimized geometry of MITPIM were scaled [31] by using 0.9682 factor for frequencies above 1700 cm^{-1} and by using 1.0119 factor for frequencies below 1700 cm^{-1}. TD-DFT [32], [33] approach was used to determine UV-Vis properties while GIAO approach was used to determine chemical shields for ^{1}H, ^{13}C and ^{19}F-NMR [34], [35].

2.4. *In silico* studies

2.4.1. Molecular docking simulations

Molecular docking simulations of the MITPIM and nilotinib compounds were performed by using the SwissDock online web server [36]. UCSF Chimera [37] was used for visualization of images. VEGFR2 protein (PDB ID: 2XIR) was used in the molecular docking studies. Protein Data Bank [38] was used to supply the crystal structure of the 2XIR. After the water was removed and the other residues that were not standart were eliminated from 2XIR, polar hydrogens and Kollman charges were added to 2XIR. A grid box was used to surround 2XIR's active site residues. The 3D coordinates that was binding side of protein were determined by using DeepSite module [39]. By also adding Gasteiger charges to MITPIM and nilotinib which were calculated optimized geometries, were used in the moleculer docking studies.

2.4.2. ADMEt predictions

Physicochemical, pharmacokinetic, lipophilicity, and drug similarity properties of newly synthesized MITPIM were calculated using the SwissADME

online platform [40]. The toxicity parameters such as LD50 and the acceptable usage range of MITPIM were identified using the ProTox-II online server [41].

3. Results and Discussion

3.1. NMR spectra

To make it simpler to compare experimental and computed chemical shifts of the MITPIM, all acquired values are shown collectively in **Table 1**. The computed chemical shift value of the hydroxyl proton of MITPIM was lower as compared to the experimental result (experimental value: 12.50 ppm, theoretical value: 4.53 ppm). While the protons of the methyl group as a doublet peak were at 2.31 ppm experimental, they were at 2.26-2.08 ppm theoretical. Whilst chemical shift values of aromatic protons were observed experimentally in the range of 6.99-8.66 ppm, the DFT technique predicted that they would be in the range of 6.83-9.03 ppm. The results show that the theoretical analysis accurately discloses the characteristics of the MITPIM compound and confirms the spectrum data quite well. **Figures 2** and **3** show, respectively, the compound's experimentally obtained and theoretically predicted ^{1}H-NMR spectra.

Table 1. Experimentally and theoretically obtained ^{1}H-NMR ($CDCl_3$) chemical shifts ($CDCl_3$)

Proton Number	Experimental chemical shift (ppm)	Theoretical chemical shift (ppm)
H9	8.66 (s, 1H)	9.03
H13	7.85 (s, 1H)	8.50
H4	7.51 (s, 1H)	8.10
H6	7.47 – 7.38 (m, 4H)	7.76
H7		7.58
H11		7.52
H5		7.40
H12, H8	7.05 (dd, *J* = 8.7, 0.6 Hz, 1H) 7.09 (s, 1H)	7.11
H10	6.99 (td, *J* = 7.5, 1.0 Hz, 1H)	6.83
H14	12.50 (s, 1H)	4.53
H2, H3	2.31 (d, *J* = 0.9 Hz, 3H)	2.26 2.08
H1		

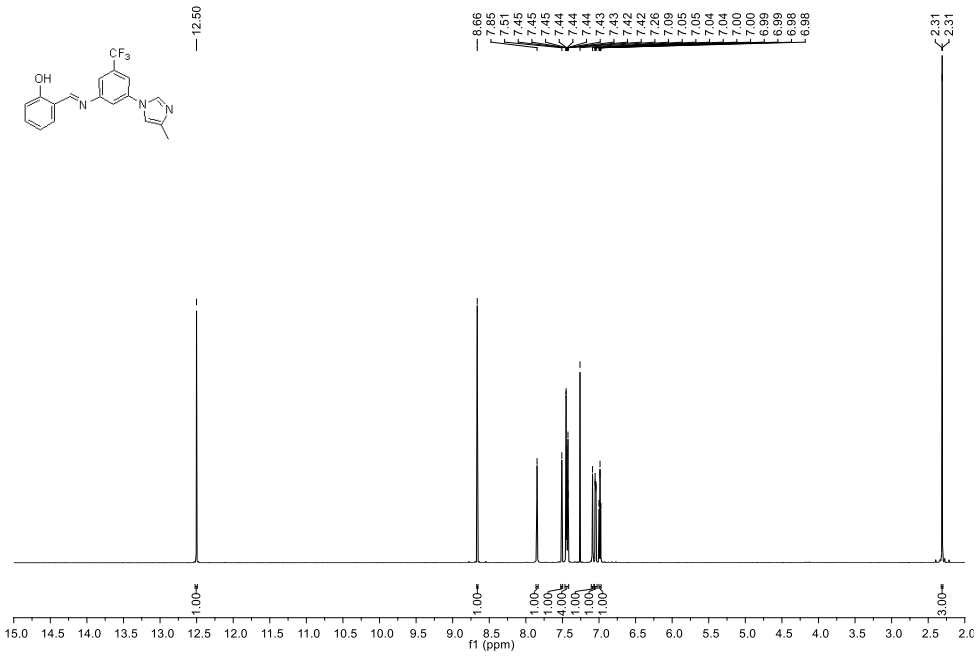

Figure 2. Experimental ^{1}H-NMR spectrum taken in $CDCl_3$ of the MITPIM

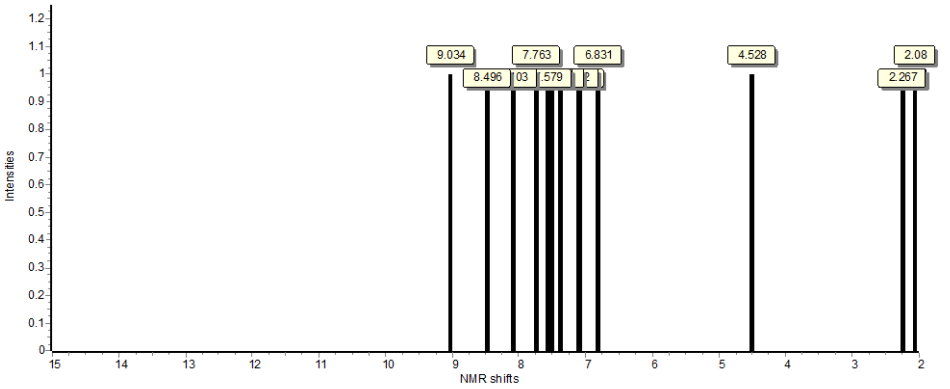

Figure 3. Theoretical ^{1}H-NMR spectrum taken in $CDCl_3$ of the MITPIM

In the ^{13}C-NMR spectrum, the C13 atom associated with the O-H group was measured and recorded at 161.18, however in the theoretical spectrum, this signal was discovered at 164.0 ppm. The signal for the methyl group's carbon atom C1 was identified at 13.65 ppm, while the calculated chemical shift for it appeared at 14.07. The carbon atom C18 of the trifluoromethyl group gave the quartet signals at 125.44, 123.89, 122.34, and 120.79 ppm, and this carbon atom signal was discovered at 132.80 ppm in the theoretical spectrum. The Schiff base's carbon atom C11 produced a signal at 165.34 ppm, and this carbon atom signal was found in the theoretical spectrum at 161.10 ppm. The expected region was where all other carbon atoms were seen, and **Table 2** was given a detailed breakdown of the values that resulted. **Figures 4** and **5** show the compound's theoretically predicted and experimentally acquired ^{13}C-NMR spectra.

Table 2. Experimentally and theoretically obtained ^{13}C-NMR ($CDCl_3$) chemical shifts

Carbon Number	Group	Experimental chemical shift (ppm)	Theoretical chemical shift (ppm)
C1	CH_3	13.65	14.07
C2	CH	134.42	135.84
C3	C	140.51	146.09

C4	CH	114.28	114.65
C5	C	133.81 133.62 133.43 133.24	138.14
C6	CH	115.35 115.34	112.01
C7	C	138.90	142.15
C8	CH	117.49	119.77
C9	C	151.01	161.21
C10	CH	116.03, 116.00	114.58
C11	CH	165.34	161.10
C12	C	118.55	125.78
C13	C	161.18	164.00
C14	CH	117.10	117.69
C15	CH	134.49	138.97
C16	CH	119.54	123.87
C17	CH	132.94	132.12
C18	CF_3	125.44 123.89 122.34 120.79	132.80

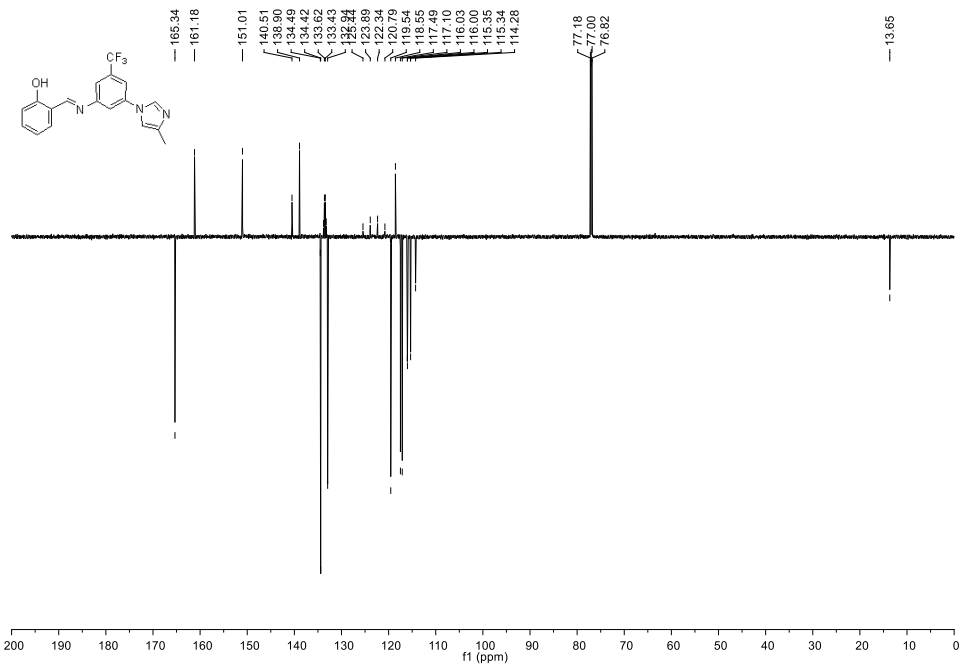

Figure 4. Experimental ^{13}C-NMR spectrum taken in $CDCl_3$ of the MITPIM

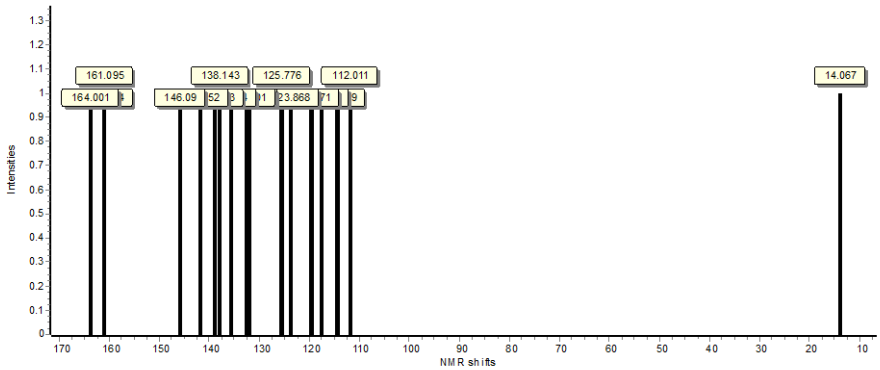

Figure 5. Theoretical ^{13}C-NMR spectrum taken in $CDCl_3$ of the MITPIM

In order to confirm MITPIM's structure ^{19}F-NMR analyses was also done. Experimental measurements at -57.85 ppm revealed the fluorine atoms as singlet peak. Theoretically, the relevant atoms were calculated to range between -66.77 and -99.08 ppm using C_6F_6 as a reference. To calculate theoretical chemical shifts of MITPIM, $\delta = \sigma_{ref} - \sigma + \delta_{ref}$ (σ_{ref} = 333.6 ppm, δ_{ref} = -164.9 ppm, σ = calculated shift) equation was used [42]. The data were shown in Table **3**, experimental and theoretical spectra were given in **Figures 6** and **7**

Table 3. Experimentally and theoretically obtained ^{19}F-NMR chemical shifts

Fluorine Number	Experimental chemical shift (ppm)	Theoretical chemical shift (ppm)
F1	-57.85 (CF_3)	-66.77
F2		-68.91
F3		-99.08

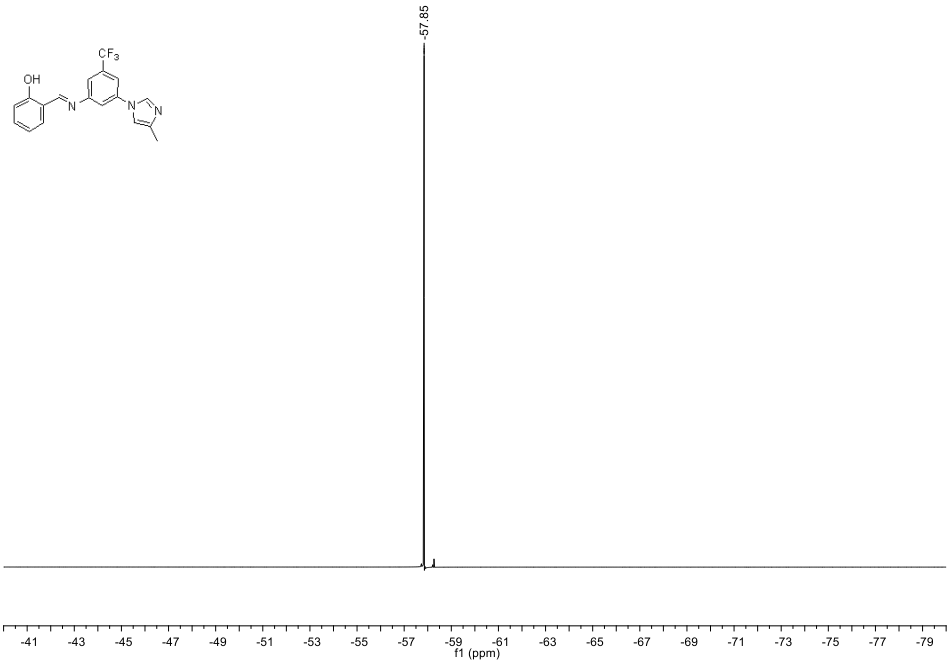

Figure 6. Experimental ^{19}F-NMR ($CDCl_3$) spectrum of the MITPIM

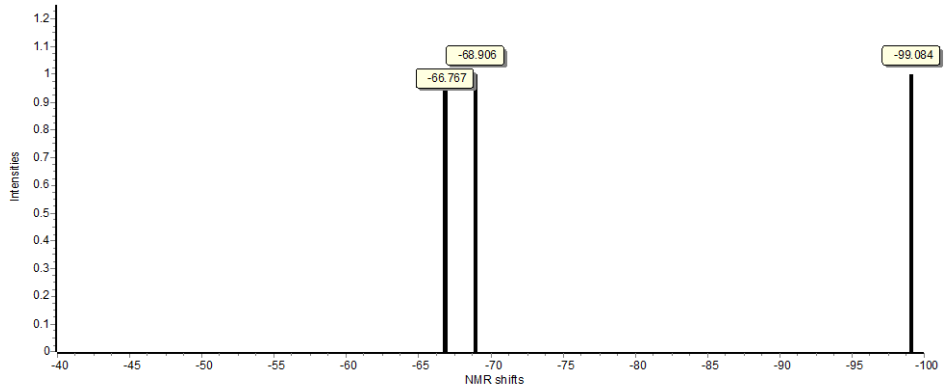

Figure 7. Theoretical ^{19}F-NMR ($CDCl_3$) spectrum of the MITPIM

A correlation between theoretical and experimental NMR chemical shift values was examined, and it was found that theoretical predictions and experimental data showed a good agreement [25], [43–45].

3.2. FT-IR spectra

Table 4 displayed all FT-IR frequency comparisons between the observed and predicted values for each constituent. The C=N double bond stretching vibration was discovered at 1600/1646 cm^{-1} in the experimental/theoretical FT-IR spectra of the molecule that were captured on the KBr disc. The compound showed the stretching vibration of the -OH group as a broad band at 3360 cm^{-1}, which is consistent with the estimated vibrational frequency of 3350 cm^{-1}.

Table 4. Experimentally and theoretically Vibration frequencies ($\tilde{\nu}_{max}$ (cm^{-1})) of MITPIM

	Vibration frequencies ($\tilde{\nu}_{max}$ (cm^{-1}))	
Vibrational band	**Theoretical**	**Experimental**
O-H stretching	3350	3360
C-H stretching	3185	3191
C-H stretching	3120	3117
C-H stretching	2934	2926
C=N stretching	1646	1600
C-N stretching	1323	1323
C-N stretching	1287	1284
C-F stretching	1186	1175

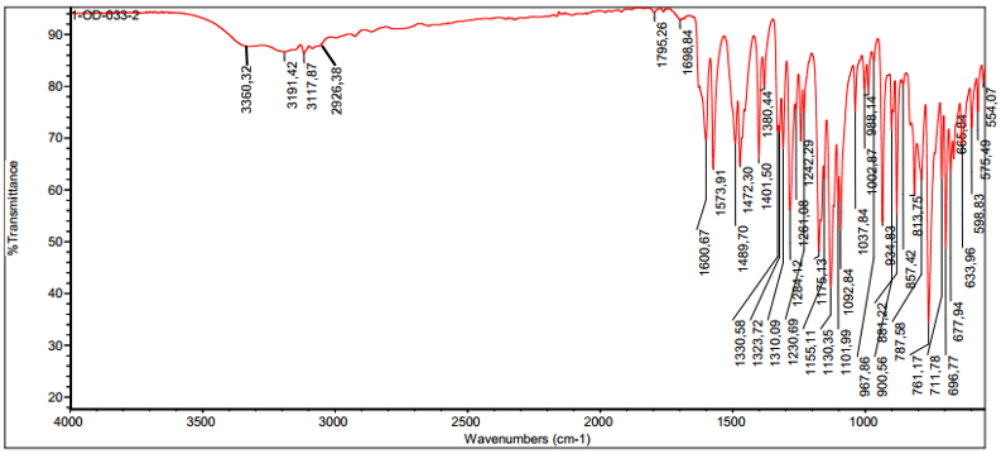

Figure 8. Experimental FT-IR spectrum of the MITPIM

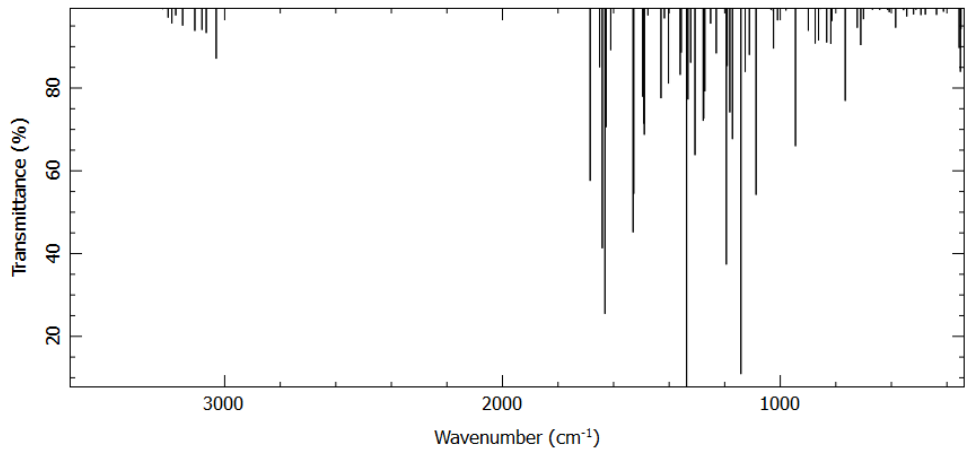

Figure 9. Theoretical FT-IR spectrum of the MITPIM

Figure 10 showed the linearity between the theoretical and experimental frequency of the compound and the equality of y = 1.0078x – 24.352 (R^2 = 0.9997) was discovered. These results showed that there was agreement between the theoretically and empirically established frequency values [25].

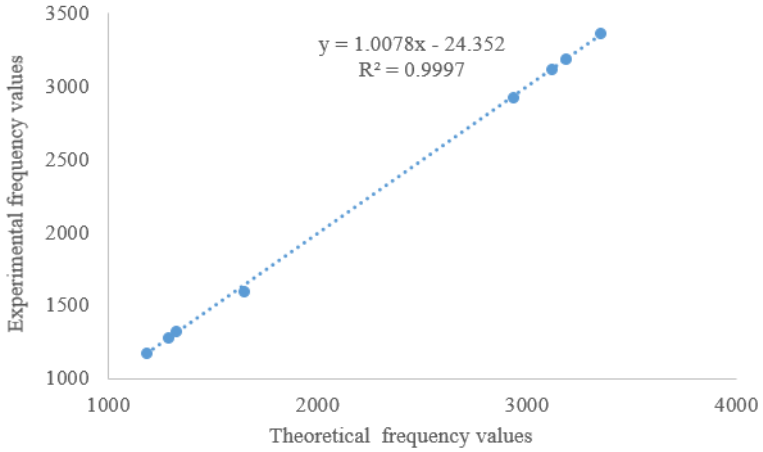

Figure 10. The linearity of frequency values (cm^{-1})

3.3. UV-Vis spectrum and frontier molecular orbitals

The UV-Vis spectra of MITPIM in $CHCl_3$ were taken between 200 and 700 nm. We computed the electronic transition wavelengths of the compounds using the TD-DFT method and the B3LYP/6-311G(d,p) level. **Figure 11** displays the UV-Vis spectra of the compounds in both experimental and theoretical forms. Also frontier molecular orbital parameters of the MITPIM (electronic transitions, excitation energies (eV) and oscillator strengths (f)) were shown in **Table 5.** It is shown that in **Table 5,** MITPIM had three maximum absorbance (λ) bands experimentally. These were 344 nm, 272 nm, and 248 nm while theoretical ones were 343 nm, 293 nm, and 277 nm. The responsible band from n→π* was at 344 nm in experimental spectra while this was at 343 nm theoretically one. π→π* transition band originating from the imine group was detected at 272 nm in the experimental UV-Vis spectrum whereas it was at 293 nm in the theoretical one. The other π→π* transitions band sourced from aromatic rings of the MITPIM was at 248 nm in the experimental spectrum, while this was at 277 nm in the theoretical one.

Table 5. Experimental and theoretical electronic transitions, excitation energies (eV), oscillator strengths (f)

Compound	Transitions	Experimental		TD-DFT/B3LYP/6-311G(d,p)		
		λ (nm)	E (eV)	λ (nm)	E (eV)	f
MITPIM	n→π*	344	3.60	343	3.62	0.3311
				326		0.2860
				309		0.0139
	π→π* (imin)	272	4.56	293	4.23	0.0429
	π→π*	248	5.00	277	4.48	0.3977

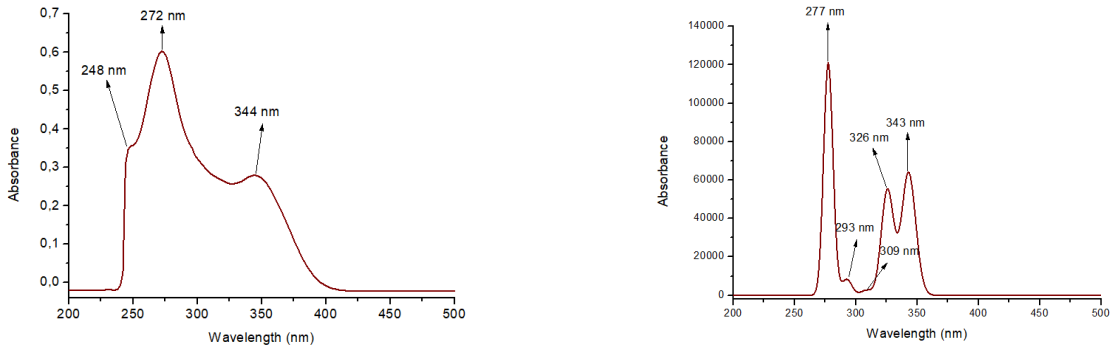

Experimental UV-Vis Spectrum Theoretical UV-Vis Spectrum

Figure 11. Experimental (left) and theoretical (right) UV-Vis spectra of the MITPIM in $CHCl_3$

The HOMO (Highest Occupied Molecular Orbital) and LUMO (Lowest Unoccupied Molecular Orbital) abbreviations are used to refer to the frontier orbitals of MITPIM. In most cases, HOMO regulates nucleophilic reactions in molecules, while LUMO regulates electrophilic reactions. The HOMOs and LUMOs of MITPIM were calculated using the DFT approach. The information in **Figure 12** related to MITPIM's molecule orbital energies, surfaces, and the energy difference between HOMO and LUMO. Analysis of the compound's HOMO-LUMO graphs revealed that HOMOs were clustered over the whole structure, whilst LUMOs were grouped on the benzene skeletons. The estimated HOMO/LUMO energy for the compound was calculated to be -6.119/-2.196 eV and the energy value for the HOMO-LUMO gap was obtained to be 4.003 eV.

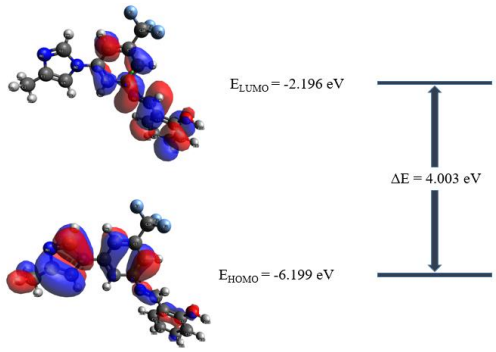

Figure 12. Surfaces of Molecular orbital, energies (E), and energy gap (ΔE) between HOMO and LUMO of the MITPIM

3.4. Computational details

3.4.1. Molecular structure

To achieve the optimized geometry for the MITPIM, a B3LYP method and 6-311G(d,p) basis set was used. The complete optimized geometry of MITPIM, including atom numbering, is shown in **Figure 13**.

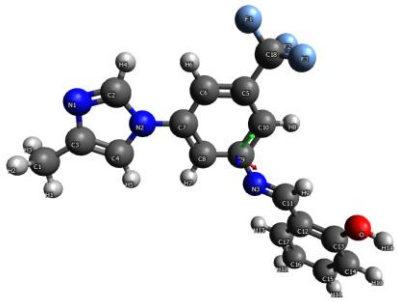

Figure 13. Optimized geometry of MITPIM by using DFT

3.4.2. Molecular electrostatic potential (MEP) diagram

Figure 14 displays the MEP surface diagram for the MITPIM computed at the DFT/B3LYP/6-311G(d,p) level. On the nitrogen atom of the imidazole moiety, the synthesized compound's MEP surface diagram showed an electron-rich area. A negative electrostatic potential was created on the nitrogen atom due to its electronegativity. These regions might be the locations of nucleophilic assaults on molecules if the synthesized molecule were to react with another molecule. The proton in the hydroxyl group, however, was the area of MITPIM electron-poor. The oxygen's high electronegativity in the hydroxyl group loosened its connection with the hydrogen atom and made the proton looser. The chemicals might behave electrophilically in these regions.

Figure 15 depicted the Mulliken atomic charge distribution for the MITPIM molecule determined by the B3LYP method using the 6-311G(d,p) basis set. It was seen that all heteroatoms have a negative charge. Due to fluorine atoms' strong electronegativity, the C18 atom was the highest positive charge (0.72681 a.u.).

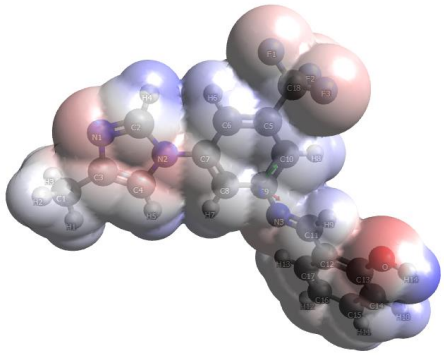

Figure 14. Calculated Molecular electrostatic potential diagram of MITPIM

After the C18 atom, H14 (0.2558 a.u.) atom was also the highest positive charge among the hydrogens due to the electronegative oxygen atom. The most negative atoms were N2 atom (-0.4373 a.u.) in imidazole and O (-0.3651 a.u.) atom in the phenol functional group. As well as N2 and O atoms, N3 (-0.3296 a.u.) atom responsible for the imin group, N1 (-0.3189 a.u.) atom in the imidazole and C5 (-0.3125 a.u.) atom in the benzene which is close to $-CF_3$ functional group had negative charges. From Mulliken charges, it was concluded that locations with high and low electron density in the MITPIM compound were compatible with the MEP diagram.

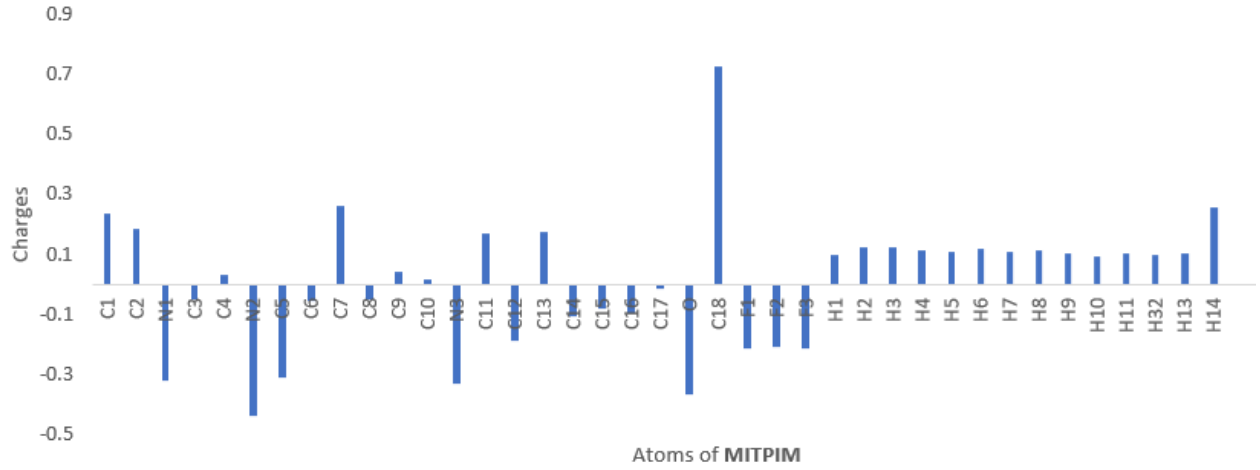

Figure 15. Calculated Mulliken atomic charges of the MITPIM

3.5. *In silico* studies

3.5.1. ADMET predictions

ADME properties of pharmacological substances are crucial in drug discovery. Physicochemical, lipophilicity, water solubility, pharmacokinetic and drug-likeness properties of new substances are important criteria in drug discovery.

Physicochemical and lipophilicity properties of substances like molecular weight, MLOGP, number of H-bond acceptors and donor atoms are the searched properties in Lipinski's rule of five. The molecular weight value of substances must be greater than 150 and less than 500. MLOGP value must be less than 4.15. The number of hydrogen bond acceptor atoms must be less than 10, Number of hydrogen bond donor atom must be less than 5. When Lipinski's rule of five was investigated in MITPIM, it was concluded that the compound has the all criteria (**Table 6**). TPSA value is also important as gets through of substances from cell membranes. The TPSA value of the substance should be less than 140 $Å^2$.

Lipophilicity is the dispersion of substances between lipids and water at specific rates. To get to their target sites, drug molecules must cross several biological membranes, including the blood-brain barrier, the skin, and the gut. So the dispersion rate is important. The consensus lipophilicity ($CLogP_{o/w}$) value of MITPIM was calculated to be 3.98.

Pharmacokinetic properties also have a crucial role in ADME properties. The Boiled-Egg model is taken part in **Figure 16** which the x-axis is TPSA and y-axis is WLOGP. While white region in the model is responsible for gastrointestinal absorption, yellow region in the model is responsible for whether the compound being crossed the blood-brain barrier or not. When the Boiled-Egg model in **Figure 16** was examined, It was concluded that the red dot was in the white region, The gastrointestinal system can easily absorb the MITPIM and the MITPIM compound did not pass the blood-brain barrier. In the pharmacokinetic properties, Cytochrome P450 enzyme systems also have a crucial role in the metabolism of taken medicines. When **Table 6** was examined, it was estimated that MITPIM is likely to be inhibited by CYP1A2, CYP2C19 and CYP2D6, while is not to be inhibited by CYP2C9 and CYP3A4.

As well as other properties, Druglikeness properties were also investigated. Lipinski (Pfizer), Ghose (Amgen), Veber (GSK), Egan (Pharmacia), and Muegge (Bayer) are the drug companies and these have various rules which are searched criteria in druglikeness properties. When **Table 6** is examined related to this field, The MITPIM compound has had all criteria except Ghose's rule because the WLogP value is greater than 5.6.

The water solubility (LogS) of a substance to reach its target is an important feature. When **Table 6** examined, LogS values of MITPIM according to various mathematical equations which were calculated by researchers are -4.68 (ESOL, Moderately soluble), -4.66 (Ali, Moderately soluble), -6.20 (SILICOS-IT, Poorly soluble) respectively.

Table 6. Physicochemical, lipophilicity, solubility, pharmacokinetics and drug-likeness properties of the MITPIM

Physicochemical Properties		**Druglikeness Properties**		
Properties	**Value**	**Requirement**	**Value**	**Compatible**
	MITPIM		**MITPIM**	**MITPIM**
		Lipinski's Rule		
Molecular Formula	$C_{18}H_{14}F_3N_3O$	MW ≤ 500	345.32	Yes
Molecular weight (MW, g/mol)	345.32	M LOGP ≤ 4.15	2.83	
Number of heavy atoms	25	HBA Atoms ≤ 10	6	
Number of aromatic heavy atoms (AHA)	17	HBD Atoms ≤ 5	1	
Number of rotatable bonds (RB)	4	**Ghose's Rule**		
Number of H-bond acceptors (HBA)	6	160 ≤ MW ≤ 480	345.32	No
Number of H-bond donors (HBD)	1	-0.4 ≤ WLOGP ≤ 5.6	5.81	
Molar Refractivity (MR)	89.25	40 ≤ MR ≤ 130	89.25	
TPSA (Å²)	50.41	20 ≤ atoms ≤ 70	39	
Lipophilicity		**Veber's Rule**		
Log $P_{o/w}$ (iLOGP)	2.93	RB ≤ 10	4	Yes
Log $P_{o/w}$ (XLOGP3)	3.90	TPSA ≤ 140	50.41	
Log $P_{o/w}$ (WLOGP)	5.81	**Egan's Rule**		
Log $P_{o/w}$ (MLOGP)	2.83	WLOGP ≤ 5.88	5.81	Yes
Consensus Log $P_{o/w}$	3.98	TPSA ≤ 131.6	50.41	
Pharmacokinetics		**Muegge's Rule**		
GI absorption	High	200 ≤ MW ≤ 600	345.32	Yes
BBB permeant	No	-2 ≤ XLOG3 ≤ 5	3.90	
P-gp substrate	No	TPSA ≤ 150	50.41	
CYP1A2 inhibitor	Yes	Number of rings ≤ 7	3	
CYP2C19 inhibitor	Yes	Number of carbon > 4	18	
CYP2C9 inhibitor	No	Number of heteroatoms > 1	4	
CYP2D6 inhibitor	Yes	RB ≤ 15	4	
CYP3A4 inhibitor	No	HBA ≤ 10	6	
Log K_p (skin permeation, cm/s)	-5.64	HBD ≤ 5	1	
Water Solubility				
Log S (ESOL) Class	-4.68 Moderately soluble			
Log S (Ali) Class	-4.66 Moderately soluble			

Log S (SILICOS-IT) Class	-6.20 Poorly soluble			

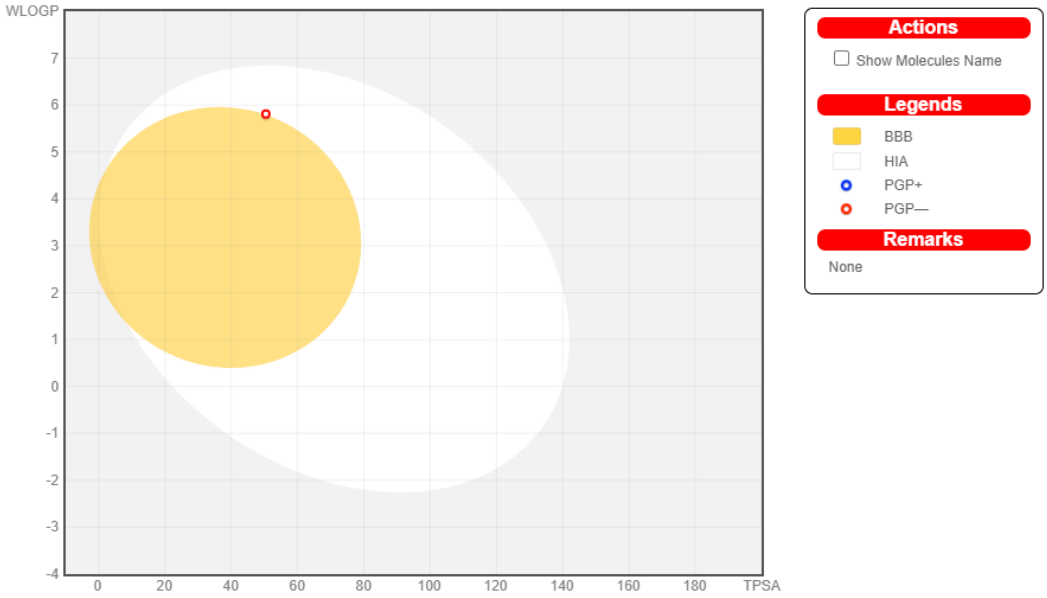

Figure 16. BOILED-Egg model of the MITPIM

The toxicity properties of MITPIM were investigated using the Protox-II online server, which is a widely used tool for predicting toxicity in chemical compounds. The lethal dose (LD50) value was determined 1000 mg/kg, based on the analysis of **Table 7**. These values were found to be lower than the corresponding value (2319.9 mg/kg) in the online server dataset. From the calculated result, It was

concluded that MITPIM exhibits some level of toxicity. Furthermore, the estimated toxicity classes for the substances were established on the Protox-II web server, which ranks compounds from the worst (class 1) to the best (class 6) based on their predicted toxicity. MITPIM was classified into the fourth

toxicity class, which indicates moderate toxicity levels. Notably, neither compound was found to exhibit any carcinogenic or mutagenic properties (**Table 7**).

Table 7. Toxicity properties of the MITPIM

Toxicity Properties	
	MITPIM
Predicted LD50	1000 mg/kg (dataset: 2319.9 mg/kg, MITPIM: 1000 mg/kg)
Predicted Toxicity Class	4
Carcinogenicity	Inactive
Mutagenicity	Inactive
Lethal Dose	Low from dataset

3.5.2. Molecular Docking Simulations

By using the VEGFR2 protein (PDB ID: 2XIR), the molecular docking simulations of MITPIM were investigated. The 3D coordinates that was binding site of the 2XIR were used as x = 21.0, y = 26.2, and z = 38.8. To create a meaningful comparison, the commercially used drug nilotinib which is a VEGFR2 inhibitor, was used. Optimized geometries of MITPIM and nilotinib were individually docked to the selected region of the 2XIR. The ligand-protein complex which has the lowest docking scores were chosen to investigate the binding modes for MITPIM and nilotinib. From molecular docking studies, valuable information such as binding energy, full fitness score, hydrogen bond location, and length values for each ligand-protein pair were obtained. These detailed findings can be found in **Table 8**.

When the binding energies of MITPIM-2XIR and Nilotinib-2XIR complexes were examined, MITPIM-2XIR binding energy was -9,34 kcal/mol and Nilotinib-2XIR binding energy was -9.69 respectively. From the results it was concluded that the bindings between ligand and proteins were exothermic, Binding energy of MITPIM-2XIR is very close to Nilotinib-2XIR.

Interactions between ligand and protein can be different types such as Van der Waals, Hydrogen bonding, etc. When the docking simulations were

examined, it was concluded that both MITPIM and nilotinib binded to ARG 1027 of 2XIR with a hydrogen bond. It was seen that the most stable interaction was between ARG 1027 HH and LIG 1 N on MITPIM-2XIR complex with 2.113 Å while to be between ARG 1027 HH and LIG 1 N on Nilotinib-2XIR complex with 2.423 Å in **Table 8**. The optimal binding positions of MITPIM-2XIR and Nilotinib-2XIR were given in **Figures 17** and **18**. Also, the hydrogen binding positions of MITPIM-2XIR and Nilotinib-2XIR were given in **Figure 19.**

Table 8. Molecular docking parameters within the ligand-target molecule couples.

Ligand-Target	ΔG (kcal/mol)	H bond Location (Length, Å)	Fullfitness score
MITPIM-2XIR	-9.34	ARG 1027 HH & LIG 1 N (2.113 Å)	-1700.32
Nilotinib-2XIR	-9.69	ARG 1027 HH & LIG 1 N (2.423 Å)	-1716.68

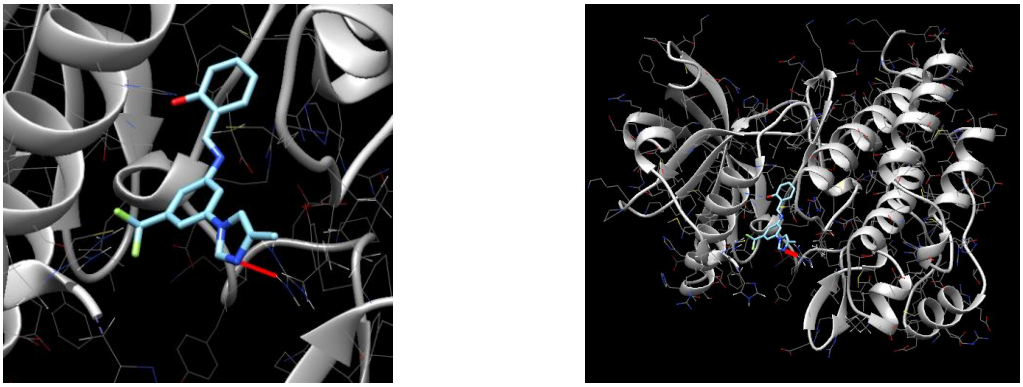

a **b**

Figure 17. Visualization of MITPIM-2XIR complex (**a**: zoom in, **b**: zoom out)

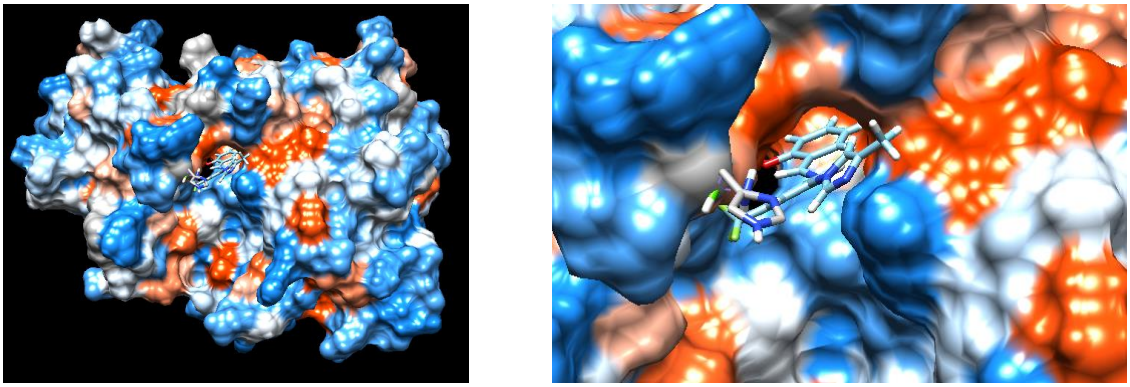

a **b**

Figure 18. The binding of the MITPIM in the cavity of 2XIR (**a**) and closer views of the hydrophobicity surface (**b**)

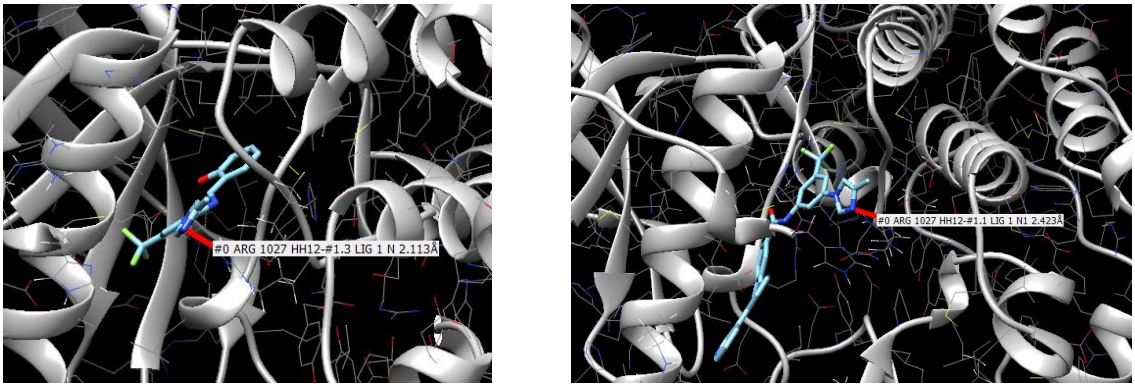

a **b**

Figure 19. H bond visulization of MITPIM (**a**) and nilotinib (**b**) to arginine aminoacid of 2XIR protein

4. Conclusion and Suggestions

Within the scope of the study 2-(((3-(4-methyl-1H-imidazol-1-yl)-5-(trifluoromethyl) phenyl)imino)methyl)phenol (MITPIM) was synthesized and characterized with spectroscopic techniques such as ^{1}H-NMR, ^{13}C-NMR, ^{19}F-NMR, UV-Vis and FT-IR. The DFT/B3LYP method and 6-311G(d,p) basis set were used to calculate all of MITPIM's spectral information. As a result of theoretical calculations, it has been seen that the values are compatible with experimental ones. The findings of *in silico* experiments that included ADME, toxicity, and molecular docking simulations revealed that the synthesized MITPIM had the potential to be a drug. Given that the mean LD50 for the MITPIM in the ProTox-II dataset was 1000 mg/kg, it is clear that this substance is either non-toxic or has very low oral toxicity. In order to forecast the possible anticancer effect of the MITPIM, molecular docking experiments were also carried out. It was shown that MITPIM and VEGFR2 (PDB ID: 2XIR) had a favorable interaction, with a binding energy of about -9.34 kcal/mol, which was near to nilotinib's binding energy of -9.69 kcal/mol. The successful outcomes show that deeper research in related fields is required for MITPIM.

The conclusion section should be stand alone. The aim of the study and its significant results should be given briefly in a concrete way. In addition, suggestions and opinions that are requested to be conveyed to the readers regarding the results of the study can be stated.

Acknowledgment

The author would like to thank Prof. Dr. Tahir TİLKİ, Prof. Dr. Bülent DEDE and Prof. Dr. Çiğdem KARABACAK ATAY for technical and theoretical support.

Contributions of the authors

Conflict of Interest Statement

Statement of Research and Publication Ethics

The study is complied with research and publication ethics

References

[1] R. L. Siegel, K. D. Miller, H. E. Fuchs, and A. Jemal, "Cancer statistics, 2022," *CA Cancer J Clin*, vol. 72, no. 1, pp. 7–33, Jan. 2022.

[2] D. T. Debela, S. G. Muzazu, K. D. Heraro, M. T. Ndalama, B. W. Mesele, D. C. Haile, S. K. Kitui, T. Manyazewal, "New approaches and procedures for cancer treatment: Current perspectives," *SAGE Open Med*, vol. 9, p. 205031212110343, Aug. 2021.

[3] V. V. Padma, "An overview of targeted cancer therapy," *Biomedicine (Taipei)*, vol. 5, no. 4, p. 19, Nov. 2015.

[4] P. Martins, J. Jesus, S. Santos, L. R. Raposoi, C. Roma-Rodrigues, P. V. Baptista, A. R. Fernandes, "Heterocyclic Anticancer Compounds: Recent Advances and the Paradigm Shift towards the Use of Nanomedicine's Tool Box," *Molecules*, vol. 20, no. 9, pp. 16852–16891, Sep. 2015.

[5] S. Kakkar, S. Kumar, B. Narasimhan, S. M. Lim, K. Ramasamy, V. Mani, S. A. A.Shah, "Design, synthesis and biological potential of heterocyclic benzoxazole scaffolds as promising antimicrobial and anticancer agents," *Chem Cent J*, vol. 12, no. 1, p. 96, Sep. 2018.

[6] T. Tahir, M. Ashfaq, M. Saleem, M. Rafiq, M. I. Shahzad, K. K. Mojzych, M. Mojzych, "Pyridine Scaffolds, Phenols and Derivatives of Azo Moiety: Current Therapeutic Perspectives," *Molecules*, vol. 26, no. 16, p. 4872, Aug. 2021.

[7] A. Verma, S. Joshi, and D. Singh, "Imidazole: Having Versatile Biological Activities," *J Chem*, vol. 2013, p. 329402, Oct. 2013.

[8] A. Abula, Z. Xu, Z. Zhu, C. Peng, Z. Chen, W. Zhu, H. A. Aisa, "Substitution Effect of the Trifluoromethyl Group on the Bioactivity in Medicinal Chemistry: Statistical Analysis and Energy Calculations," *J Chem Inf Model*, vol. 60, no. 12, pp. 6242–6250, Dec. 2020.

[9] J. B. I. Sap, N. J. W. Straathof, T. Knauber, C. F. Meyer, M. Médebielle, L. Buglioni, C. Genicot, A. A. Trabanco, T. Noël, C.W. A. Ende, and V. Gouverneur, "Organophotoredox Hydrodefluorination of Trifluoromethylarenes with Translational Applicability to Drug Discovery," *J Am Chem Soc*, vol. 142, no. 20, pp. 9181–9187, May 2020.

[10] A. S. Nair, A. K. Singh, A. Kumar, S. Kumar, S. Sukumaran, V. P. Koyiparambath, L. K. Pappachen, T. M. Rangarajan, H. Kim, and B. Mathew, "FDA-Approved Trifluoromethyl Group-Containing Drugs: A Review of 20 Years," *Processes*, vol. 10, no. 10, p. 2054, Oct. 2022.

[11] Y. Zhang, P. Cai, G. Cheng, and Y. Zhang, "A Brief Review of Phenolic Compounds Identified from Plants: Their Extraction, Analysis, and Biological Activity," *Nat Prod Commun*, vol. 17, no. 1, Jan. 2022.

[12] A. Basli, N. Belkacem, and I. Amrani, "Health Benefits of Phenolic Compounds Against Cancers," *in Phenolic Compounds - Biological Activity, InTech*, 2017, pp. 193–210, March 2017.

[13] P. G. Anantharaju, P. C. Gowda, M. G. Vimalambike, and S. V. Madhunapantula, "An overview on the role of dietary phenolics for the treatment of cancers," *Nutr J*, vol. 15, no. 1, p. 99, Dec. 2016.

[14] A. Kajal, S. Bala, S. Kamboj, N. Sharma, and V. Saini, "Schiff Bases: A Versatile Pharmacophore," *Journal of Catalysts*, vol. 2013, p. 893512, Aug. 2013.

[15] A. P. Hnatiuk, A. A. N. Bruyneel, D. Tailor, M. Pandrala, A. Dheeraj, W. Li, R. Serrano, D. A. M. Feyen, M. M. Vu, P. Amatya, S. Gupta, Y. Nakauchi, I. Morgado, V. Wiebking, R. Liao, M. H. Porteus, R. Majeti, S. V. Malhotra, M. Mercola, "Reengineering Ponatinib to Minimize Cardiovascular Toxicity," *Cancer Res*, vol. 82, no. 15, pp. 2777–2791, Aug. 2022.

[16] H. Jung, J. Kim, D. Im, H. Moon, and J.-M. Hah, "Design, synthesis, and in vitro evaluation of N-(3-(3-alkyl-1H-pyrazol-5-yl) phenyl)-aryl amide for selective RAF inhibition," *Bioorg Med Chem Lett*, vol. 29, no. 4, pp. 534–538, Feb. 2019.

[17] D. Zhu, H. Huang, D. M. Pinkas, J. Luo, D. Ganguly, A. E. Fox, E. Arner, Q. Xiang, Z. C. Tu, A. N. Bullock, A. R. Brekken, K. Ding, X. Lu, "2-Amino-2,3-dihydro-1 H -indene-5-carboxamide-Based Discoidin Domain Receptor 1 (DDR1) Inhibitors: Design, Synthesis, and in Vivo Antipancreatic Cancer Efficacy," *J Med Chem*, vol. 62, no. 16, pp. 7431–7444, Aug. 2019.

[18] H. G. Choi, P. Ren, F. Adrian, F. Sun, H. S. Lee, X. Wang, Q. Ding, G. Zhang, Y. Xie, J. Zhang, Y. Liu, T. Tuntland, M. Warmuth, P. W. Manley, J. Mestan, N. S. Gray, T.Sim "A Type-II Kinase Inhibitor Capable of Inhibiting the T315I 'Gatekeeper' Mutant of Bcr-Abl," *J Med Chem*, vol. 53, no. 15, pp. 5439–5448, Aug. 2010.

[19] M. Pandrala, A. A. N. Bruyneel, A. P. Hnatiuk, M. Mercola, and S. V. Malhotra, "Designing Novel BCR-ABL Inhibitors for Chronic Myeloid Leukemia with Improved Cardiac Safety," *J Med Chem*, vol. 65, no. 16, pp. 10898–10919, Aug. 2022.

[20] E. Kalinichenko, A. Faryna, T. Bozhok, and A. Panibrat, "Synthesis, In Vitro and In Silico Anticancer Activity of New 4-Methylbenzamide Derivatives Containing 2,6-Substituted Purines as Potential Protein Kinases Inhibitors," *Int J Mol Sci*, vol. 22, no. 23, p. 12738, Nov. 2021.

[21] X. Lu, Z. Zhang, X. Ren, X. Pan, D. Wang, X. Zhuang, J. Luo, R. Yu, K. Ding, "Hybrid pyrimidine alkynyls inhibit the clinically resistance related Bcr-AblT315I mutant," *Bioorg Med Chem Lett*, vol. 25, no. 17, pp. 3458–3463, Sep. 2015.

[22] E. Kalinichenko, A. Faryna, V. Kondrateva, A. Vlasova, V. Shevchenko, A. Melnik, O. Avdoshko and Alla Belko, "Synthesis, Biological Activities and Docking Studies of Novel 4-(Arylaminomethyl)benzamide Derivatives as Potential Tyrosine Kinase Inhibitors," *Molecules*, vol. 24, no. 19, p. 3543, Sep. 2019.

[23] E. Kalinichenko, A. Faryna, T. Bozhok, A. Golyakovich, and A. Panibrat, "Novel Phthalic-Based Anticancer Tyrosine Kinase Inhibitors: Design, Synthesis and Biological Activity," *Curr Issues Mol Biol*, vol. 45, no. 3, pp. 1820–1842, Feb. 2023.

[24] G. Faudone, R. Zhubi, F. Celik, S. Knapp, A. Chaikuad, J. Heering, D. Merk, "Design of a Potent TLX Agonist by Rational Fragment Fusion," *J Med Chem*, vol. 65, no. 3, pp. 2288–2296, Jan. 2022.

[25] Ç. K. Atay, Ö. Dilek, T. Tilki, and B. Dede, "A novel imidazole-based azo molecule: synthesis, characterization, quantum chemical calculations, molecular docking, molecular dynamics simulations and ADMET properties," *J Mol Model*, vol. 29, no. 8, p. 226, Aug. 2023.

[26] Frisch, M. J., G. W., Trucks, H. B., Schlegel, G. E., Scuseria, M. A., Robb, J. R., Cheeseman, G., Scalmani, V., Barone, G. A., Petersson, H., Nakatsuji, X., Li, M., Caricato, A., Marenich, J., Bloino, B. G., Janesko, R., Gomperts, B., Mennucci, H. P., Hratchian, J. V., Ortiz, A. F I., D. J. F. 2016. Gaussian 09, Revision E.01. Gaussian, Inc.

[27] M. D. Hanwell, D. E. Curtis, D. C. Lonie, T. Vandermeersch, E. Zurek, and G. R. Hutchison, "Avogadro: an advanced semantic chemical editor, visualization, and analysis platform," *J Cheminform*, vol. 4, no. 1, p. 17, Aug. 2012.

[28] Chemcraft - graphical software for visualization of quantum chemistry computations. Version 1.8, build 654. https://www.chemcraftprog.com [Accessed: July. 25, 2023].
[29] A. D. Becke, "Density-functional exchange-energy approximation with correct asymptotic behavior," *Phys Rev* A (Coll Park), vol. 38, no. 6, pp. 3098–3100, Sep. 1988.
[30] C. Lee, W. Yang, and R. G. Parr, "Development of the Colle-Salvetti correlation-energy formula into a functional of the electron density," *Phys Rev B*, vol. 37, no. 2, pp. 785–789, Jan. 1988.
[31] J. P. Merrick, D. Moran, and L. Radom, "An Evaluation of Harmonic Vibrational Frequency Scale Factors," *J Phys Chem A*, vol. 111, no. 45, pp. 11683–11700, Oct. 2007.
[32] R. Bauernschmitt and R. Ahlrichs, "Treatment of electronic excitations within the adiabatic approximation of time dependent density functional theory," *Chem Phys Lett*, vol. 256, no. 4–5, pp. 454–464, Jul. 1996.
[33] M. E. Casida, C. Jamorski, K. C. Casida, and D. R. Salahub, "Molecular excitation energies to high-lying bound states from time-dependent density-functional response theory: Characterization and correction of the time-dependent local density approximation ionization threshold," *J Chem Phys*, vol. 108, no. 11, pp. 4439–4449, Mar. 1998.
[34] R. Ditchfield, "Molecular Orbital Theory of Magnetic Shielding and Magnetic Susceptibility," *J Chem Phys*, vol. 56, no. 11, pp. 5688–5691, Jun. 1972.
[35] K. Wolinski, J. F. Hinton, and P. Pulay, "Efficient implementation of the gauge-independent atomic orbital method for NMR chemical shift calculations," *J Am Chem Soc*, vol. 112, no. 23, pp. 8251–8260, Nov. 1990.
[36] A. Grosdidier, V. Zoete, and O. Michielin, "SwissDock, a protein-small molecule docking web service based on EADock DSS," *Nucleic Acids Res*, vol. 39, no. suppl, pp. W270–W277, Jul. 2011.
[37] E. F. Pettersen et al., "UCSF Chimera--A visualization system for exploratory research and analysis," *J Comput Chem*, vol. 25, no. 13, pp. 1605–1612, Oct. 2004.
[38] H. M. Berman, J. Westbrook, Z. Feng, G. Gilliland, T. N. Bhat, H. Weissig, I. N. Shindyalov, P. E. Bourne, "The Protein Data Bank," *Nucleic Acids Res*, vol. 28, no. 1, pp. 235–242, Jan. 2000.
[39] J. Jiménez, S. Doerr, G. Martínez-Rosell, A. S. Rose, and G. De Fabritiis, "DeepSite: protein-binding site predictor using 3D-convolutional neural networks," *Bioinformatics*, vol. 33, no. 19, pp. 3036–3042, Oct. 2017.
[40] A. Daina, O. Michielin, and V. Zoete, "SwissADME: a free web tool to evaluate pharmacokinetics, drug-likeness and medicinal chemistry friendliness of small molecules," *Sci Rep*, vol. 7, no. 1, p. 42717, Mar. 2017.
[41] P. Banerjee, A. O. Eckert, A. K. Schrey, and R. Preissner, "ProTox-II: a webserver for the prediction of toxicity of chemicals," *Nucleic Acids Res*, vol. 46, no. W1, pp. W257–W263, Jul. 2018.
[42] B. Raimer, P. G. Jones, and T. Lindel, "Quantum chemical calculation of ^{19}F NMR chemical shifts of trifluoromethyl diazirine photoproducts and precursors," *J Fluor Chem*, vol. 166, pp. 8–14, Oct. 2014.
[43] Ç. K. Atay, Y. Kara, M. Gökalp, I. Kara, T. Tilki, and F. Karci, "Disazo dyes containing pyrazole and indole moieties: Synthesis, characterization, absorption characteristics, theoretical calculations, structural and electronic properties," *J Mol Liq*, vol. 215, pp. 647–655, Mar. 2016.
[44] M. Gökalp, T. Tilki, and Ç. K. Atay, "Newly Synthesized Aminothiazole Based Disazo Dyes and Their Theoretical Calculations," *Polycycl Aromat Compd*, pp. 1–23, Feb. 2023.
[45] B. Sezgin, T. Tilki, Ç. K. Atay, and B. Dede, "Comparative in vitro and DFT antioxidant studies of phenolic group substituted pyridine-based azo derivatives," *J Biomol Struct Dyn*, vol. 40, no. 11, pp. 4921–4932, Jul. 2022.